NASA TECHNICAL NOTE

NASA TN D-5721

c. 1

NASA TN D-5721

SHOCK-WAVE SHAPES AND SURFACE PRESSURES ON HEMISPHERE- AND CONE-CYLINDERS IN LOW-DENSITY HYPERSONIC FLOW INCLUDING ABLATION

by Daryl J. Monson and Donald M. Kuehn

Ames Research Center
Moffett Field, Calif.

NATIONAL AERONAUTICS AND SPACE ADMINISTRATION • WASHINGTON, D. C. • APRIL 1970

1. Report No. NASA TN D-5721	2. Government Accession No.	3. Recipient's Catalog No.
4. Title and Subtitle SHOCK-WAVE SHAPES AND SURFACE PRESSURES ON HEMISPHERE- AND CONE-CYLINDERS IN LOW-DENSITY HYPERSONIC FLOW INCLUDING ABLATION		5. Report Date April 1970 6. Performing Organization Code
7. Author(s) Daryl J. Monson and Donald M. Kuehn		8. Performing Organization Report No. A-3499
9. Performing Organization Name and Address NASA Ames Research Center Moffett Field, Calif. 94035		10. Work Unit No. 129-01-02-11-00-21 11. Contract or Grant No.
12. Sponsoring Agency Name and Address National Aeronautics and Space Administration Washington D. C. 20546		13. Type of Report and Period Covered Technical Note 14. Sponsoring Agency Code
15. Supplementary Notes		

16. Abstract

Shock-wave shapes and surface pressures were determined in air for highly cooled hemisphere- and cone-cylinders with and without ablating noses. The test Mach number was 14. The test Reynolds numbers of 9000 and 1000, based on the cylinder diameter, were estimated to be in the boundary-layer and merged-layer flow regimes, respectively. Comparisons with the predictions of viscous-interaction theory have been made and the range of validity for the theory has been assessed.

The results show that in the merged-layer regime viscous-interaction theory can predict the shock-wave shapes for these bodies but fails to predict the surface pressures on the bodies. With merging, the surface pressures on the hemisphere-cylinder decreased below the predicted inviscid pressures. The behavior of the shock waves and surface pressures for these bodies in the merged-layer regime is qualitatively the same as that previously observed for sharp bodies.

Nose ablation displaced the shock waves outward and increased the surface pressures on the bodies for a short distance behind the noses. These trends were qualitatively predicted by viscous-interaction theory.

17. Key Words Suggested by Authors Shock waves Pressure distribution Ablation Low density flow Hypersonic flow	18. Distribution Statement Unclassified - Unlimited

19. Security Classif. (of this report)	20. Security Classif. (of this page)	21. No. of Pages	22. Price*
Unclassified	Unclassified	17	$3.00

*For sale by the Clearinghouse for Federal Scientific and Technical Information
Springfield, Virginia 22151

SYMBOLS

A	$\frac{\pi d^2}{4}$
C	Chapman-Rubesin viscosity coefficient
d	cylinder diameter
$\dot{m}$	rate of total mass ablated from a nose
M	Mach number
p	pressure
r	coordinate normal to the cylinder axis measured from the axis
Re	Reynolds number
u	velocity component parallel to the x-axis
$\overline{V}$	rarefaction parameter, $M_\infty\left(\frac{C}{Re_{\infty,b}}\right)^{1/2}$
x	coordinate parallel to the cylinder axis measured from the nose-cylinder junction
ρ	density

Subscripts

b	nose radius of a blunt body
d	cylinder diameter
t_2	total condition behind a normal shock wave
w	wall condition
∞	free-stream condition

SHOCK-WAVE SHAPES AND SURFACE PRESSURES ON HEMISPHERE- AND CONE-CYLINDERS IN LOW-DENSITY HYPERSONIC FLOW INCLUDING ABLATION

Daryl J. Monson and Donald M. Kuehn

Ames Research Center

SUMMARY

Shock-wave shapes and surface pressures were determined in air for highly cooled hemisphere- and cone-cylinders with and without ablating noses. The test Mach number was 14. The test Reynolds numbers of 9000 and 1000, based on the cylinder diameter, were estimated to be in the boundary-layer and merged-layer flow regimes, respectively. Comparisons with the predictions of viscous-interaction theory have been made and the range of validity for the theory has been assessed.

The results show that in the merged-layer regime viscous-interaction theory can predict the shock-wave shapes for these bodies but fails to predict the surface pressures on the bodies. With merging, the surface pressures on the hemisphere-cylinder decreased below the predicted inviscid pressures. The behavior of the shock waves and surface pressures for these bodies in the merged-layer regime is qualitatively the same as that previously observed for sharp bodies.

Nose ablation displaced the shock waves outward and increased the surface pressures on the bodies for a short distance behind the noses. These trends were qualitatively predicted by viscous-interaction theory.

INTRODUCTION

The flow over sharp flat plates, wedges, and cones successively enters the boundary-layer, weak- and strong-interaction, and merged-layer regimes as the rarefaction of the flow increases. Viscous-interaction theories (e.g., ref. 1) have been shown to predict the shock-wave locations on these bodies in all the regimes (ref. 2) but to overpredict the measured surface pressures in the merged-layer regime (e.g., refs. 2, 3, and 4). McCroskey, et al. (ref. 5), attribute this failure to a departure from a Rankine-Hugoniot shock wave when the boundary layer merges with the shock wave.

Probstein (ref. 6) classified the flow over blunt bodies into two regimes. The first includes the boundary-layer, vorticity-interaction, and viscous-layer regimes; the second includes the incipient merged-layer and fully merged-layer regimes. In this report they shall be referred to as the

boundary-layer and merged-layer regimes, respectively. The usual viscous-interaction theory for blunt bodies numerically calculates the boundary-layer displacement thickness over a body, adds this to the body thickness, and calculates the inviscid pressures on the "new" body shape. The theory has successfully predicted surface pressures on a variety of blunt bodies in the boundary-layer regime (e.g., refs. 7, 8, and 9). There are indications that the theory may fail at low densities, however. Marchand, et al. (ref. 7), substantially overpredicted pressures on a highly cooled, slender blunt cone that may have been in the merged-layer regime, and were unable to offer an explanation for the disagreement. Kuehn (ref. 10) measured pressures that agreed with inviscid theory for highly cooled hemisphere- and cone-cylinders at conditions that may have been merged. He attributed the lack of viscous induced pressures to wall cooling which resulted in a negligible displacement thickness of the boundary layer over the bodies. Thus, at least for surface pressures, viscous-interaction theories appear to fail for blunt bodies at low densities just as they do for sharp bodies. Questions remain, however, on when and for what reason this failure will occur, and whether it will also occur for other properties such as shock-wave shapes.

In this report, the results of an experimental investigation of the shock-wave shapes and surface pressures for ablating and highly cooled non-ablating hemisphere- and cone-cylinders in low-density hypersonic flow are presented and compared with predictions made by simple viscous-interaction theories. The data were obtained as part of a larger study of flow separation ahead of flares on a cylinder (ref. 11). In reference 11, the attached-flow pressure data were used in determining flow separation and were not analyzed in themselves, as is done in the present study. The experiments were conducted at a Mach number of 14 and at Reynolds numbers of 9000 and 1000 based on the cylinder diameter. The purpose of the report is threefold: to present measured surface pressures and shock-wave shapes for two highly cooled blunt bodies at conditions in the boundary-layer and merged-layer regimes; to compare the results with predictions from viscous-interaction theory, and examine under what conditions and for what reasons the theory fails; and to give some preliminary indications of the effects of nose ablation on the surface pressures and shock-wave shapes.

EXPERIMENTAL TECHNIQUE

Test Facility and Conditions

The experiments were performed in the Ames Entry Aerodynamics Tunnel sketched in figure 1. The nominal test Mach number, based on pitot-pressure surveys and nonequilibrium nozzle calculations (ref. 12), was 14. The test-stream calibration showed a centerline Mach number gradient of 1.8×10^{-2} per cm. Additional facility and stream calibration details are given in reference 11. The present investigation was conducted at two conditions: (1) at a reservoir pressure of 67 atmospheres, a total enthalpy of 4.2×10^{6} J/kg, and a Reynolds number, $Re_{\infty,d}$, of 9000; and (2) at a reservoir pressure of 10 atmospheres, a total enthalpy of 8.2×10^{6} J/kg, and a Reynolds number, $Re_{\infty,d}$, of 1000.

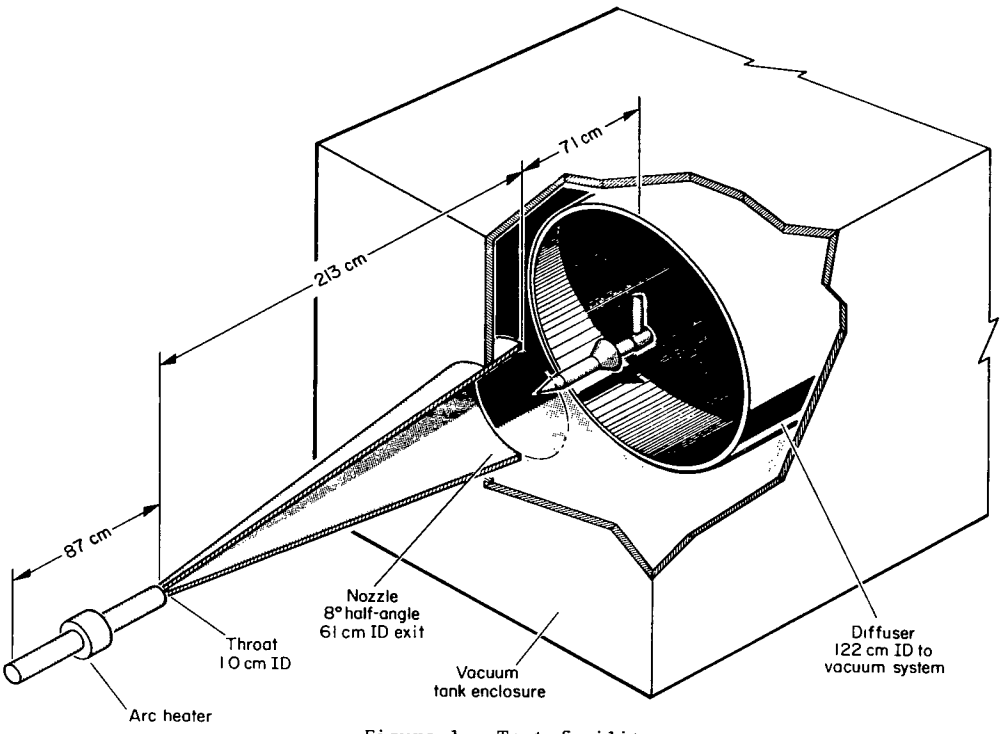

Figure 1.- Test facility.

Models

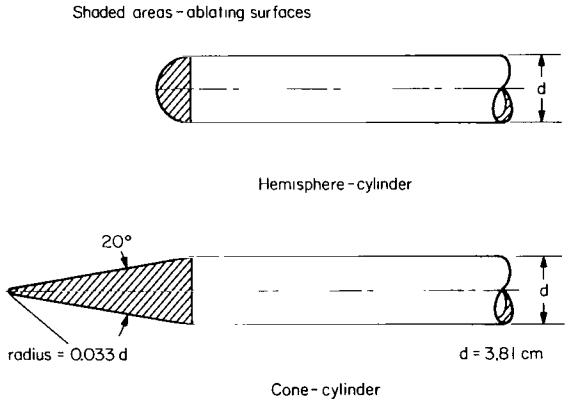

Figure 2.- Test models.

The model configurations used in these tests are shown in figure 2. The cylinder was thick-walled stainless steel, the nonablating noses were copper, and the ablating noses were Teflon, Delrin, and high-density phenolic nylon. The static-pressure orifices (dia. = 0.24 cm) were located along the cylinder with a longitudinal spacing of 0.57 cm. Thin-walled, 0.46 cm i.d. stainless-steel tubing connected the orifices to pressure cells located 2 meters from the model. The models were protected by a retractable shield while the tunnel was started.

Surface Pressure, Shock-Wave Shape, and Ablation-Rate Measurements

Surface pressures were measured with capacitance-type pressure cells to an accuracy of 5 percent at the lowest pressures measured (30 μ Hg) and to 1 percent at the highest pressures (1000 μ Hg). Pre-run out-gassing procedures

eliminated pressure gradients in the lines, and during a run, the pressures were allowed to reach equilibrium (typically within 20-40 sec) before data were taken. The measured pressures were corrected for longitudinal test-stream gradients (ref. 13) and low-density orifice effects (ref. 14). The orifice corrections ranged from 0 percent near the shoulder of the hemisphere-cylinder to 77 percent far downstream on the cone-cylinder at $Re_{\infty,d} = 1000$, and resulted in scaling the measured pressures upward. The latter corrections were made using wall heat-transfer rates calculated by a boundary-layer program to be discussed later. For the present highly cooled bodies, the corrections are insensitive to the heat transfer. The same boundary-layer calculations predicted surface shear stresses that were, in all cases, less than the local pressure, thus allowing Potter's method to be applied. The low-density effects on stagnation pressure (ref. 15) and the effects of temperature gradients along the pressure lines (ref. 16) were negligible.

Shock-wave shapes were measured from photographs of the natural luminescent flow field around the models during the runs. The photographs are not included in this report because the shock waves were not visible in the reproductions. This method was used because normal visualization techniques, such as schlieren, are not adequate at the low densities encountered. Pitot-pressure surveys verified that the shock wave over the cylindrical portion of the models was located where the luminescence changed intensity. The measured shock-wave shapes were corrected for the longitudinal test-stream gradients (ref. 13).

Ablation rates for the ablating noses were obtained by weighing the models before and after a run and dividing the difference by the run time corrected for the estimated starting time for ablation. Quoted rates are averages of these values, usually over several runs of various durations. The rates should be considered as only approximate since the materials may not have ablated at a constant rate during the runs, and the phenolic nylon and Delrin were observed to lose an unknown fraction of their mass by melt. To achieve ablation rates as close to steady state as possible, data for the ablating bodies were taken after about 30 seconds of run time. In some cases, the Delrin noses were blunted considerably by the end of a run.

RESULTS AND DISCUSSION

Flow Regimes

The flow regimes over the noses of the test models may be classified according to the criterion of Ahouse and Harbour (ref. 17) that merging for blunt bodies occurs for $\overline{V} > 0.3$. For the hemisphere-cylinder model, the lower Reynolds number test condition corresponds to $\overline{V} = 0.47$; the other to $\overline{V} = 0.17$. This clearly puts the nose of this configuration in the boundary-layer regime at $Re_{\infty,d} = 9000$ and in the merged-layer regime at $Re_{\infty,d} = 1000$. Application of the above criterion to the cone-cylinder model indicates that the blunt tip is merged at both conditions. Classification of the flow downstream of the noses is discussed below.

The just described classifications are consistent with the behavior of the ablation vapors that were observed during testing (see photographs in ref. 11). The vapors should diffuse approximately as far out as the boundary-layer edge on a body (ref. 18). At $Re_{\infty,d} = 9000$, the vapors filled one-third to one-half of the shock layer over the cylinder for both bodies. At $Re_{\infty,d} = 1000$, the vapors completely filled the shock layer on both bodies as far back as two or three cylinder diameters from the nose-cylinder junction. Thus, it is concluded that both bodies are in the boundary-layer regime at $Re_{\infty,d} = 9000$ and in the merged-layer regime at $Re_{\infty,d} = 1000$.

Shock-Wave Shapes

The measured shock-wave shape data are presented in figures 3 and 4, together with the predicted inviscid and viscous induced shock shapes. Measurements were not always possible near the nose because the film contrast was insufficient to show the shock waves. For some cases, this may have been due to merging of the shock wave and viscous layer resulting in a "shock" that is thick and diffuse.

The inviscid shock waves were obtained with a perfect-gas blunt-body and characteristics program of Inouye, et al. (ref. 19). The perfect-gas assumption was justified by nonequilibrium blunt-body calculations derived by a program of Garr and Marrone (ref. 20), which predicted frozen shock layers around the bodies at both test conditions.

The viscous induced shock wave for each model was obtained by calculating boundary-layer displacement thickness over the nose using a perfect-gas boundary-layer program of Clutter and Smith (ref. 21), adding this thickness to the geometric nose thickness, and calculating the inviscid flow field around the "new" nose. The boundary layer on the cylinder cannot affect the shock-wave shape in the region of interest since characteristic waves originating on the cylinder cannot reach the shock wave for several diameters downstream of the nose for either body. The edge conditions used in the boundary-layer program were the inviscid wall values. Refinements in these conditions were not felt to be justified since the application of boundary-layer theory to the present low densities is questionable. To calculate boundary layers for the ablating noses the total measured mass-injection rates were matched and the distributions of mass injection and surface temperature were estimated from the predicted nonablating heating-rate distributions and materials data from references 22 and 23, and unpublished data from Winovich. The molecular weights of the ablation vapors were not matched, since the program assumed air-into-air injection. (From the above references, the molecular weights of Teflon, Delrin, and phenolic nylon are 100, 15, and 18, respectively. Since the molecular weight of Teflon differs considerably from that for air, calculations are not presented for it in this report.) Displacement thicknesses for the ablating cases were calculated according to the definition of Hayasi (ref. 24) for boundary layers with blowing.

The nonablating shock-wave shape data in figure 3 show that the shock wave for the hemisphere-cylinder is independent of Reynolds number for both test conditions, whereas the shock wave for the cone-cylinder is displaced

outward at both conditions with the greater amount occurring at the lowest Reynolds number. These effects are consistent with the boundary-layer calculations which show that the displacement thickness over the cooled hemisphere is always negligible, but on the cone is significant at both conditions and largest at the lower Reynolds number. The calculated shock-wave shapes agree well with the measured results. The agreement with theory into the merged-layer regime is similar to that previously observed for sharp flat plates and wedges.

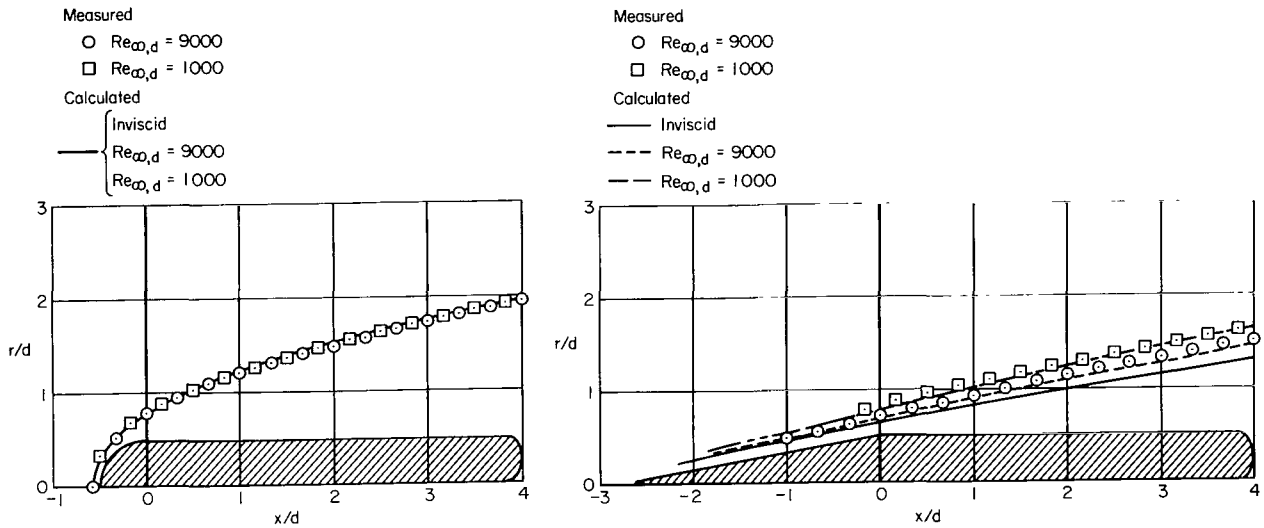

(a) Hemisphere-cylinder.

(b) Cone-cylinder.

Figure 3.- The shock shapes for the nonablating bodies; M_∞ = 14.

The shock-wave-shape data in figure 4 show that for ablating noses that ablation causes an outward movement of the shock wave. This is understandable since calculations show that ablation increases the boundary-layer displacement thickness on the nose for all cases. The extent of displacement varies considerably, however, and may be influenced by Reynolds number, ablation rate, ablation-gas molecular weight, and surface temperature. Since these all vary together, their individual effects cannot be separated from the data. The viscous-interaction calculations, which include the effects of all the variables except molecular weight, are observed to predict the shock positions adequately for the phenolic-nylon noses at both test conditions. Calculations were not made for the other ablation materials.

Surface Pressures

The measured surface-pressure data are presented in figures 5 and 6 along with the predicted inviscid and viscous induced pressures. Measurements were not always obtained near the shoulder since they were not needed in the original separation study in which the present data were obtained. Inviscid pressures and viscous induced pressures labelled "present method" were obtained as previously discussed for the theoretical shock-wave shapes by

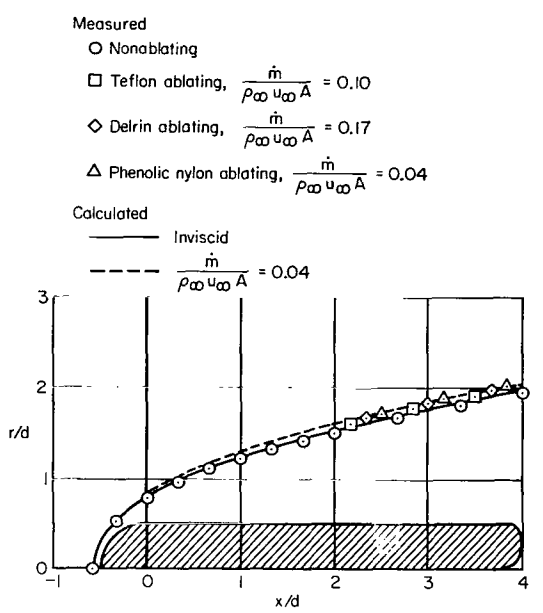

(a) Hemisphere-cylinder, $Re_{\infty,d}$ = 9000.

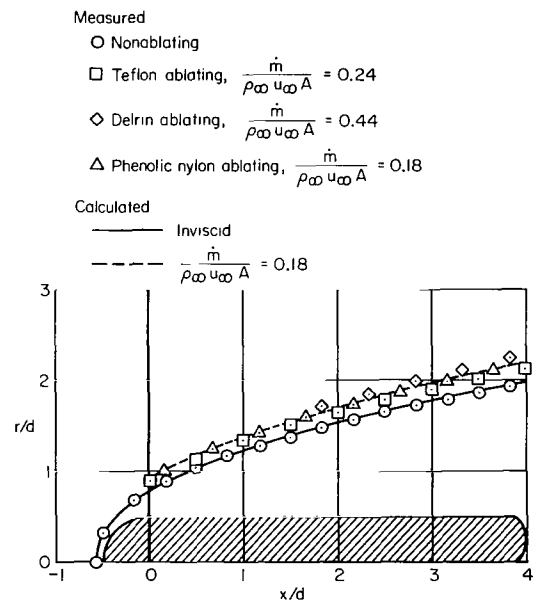

(b) Hemisphere-cylinder, $Re_{\infty,d}$ = 1000.

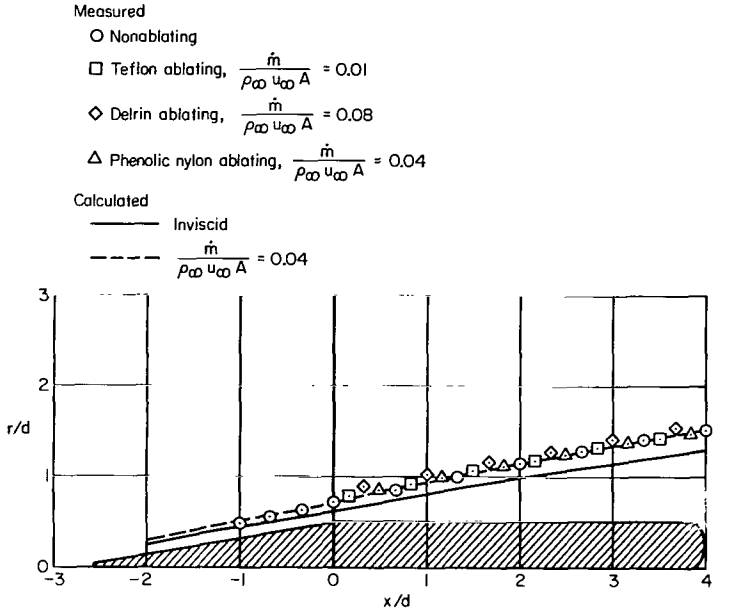

(c) Cone-cylinder, $Re_{\infty,d}$ = 9000.

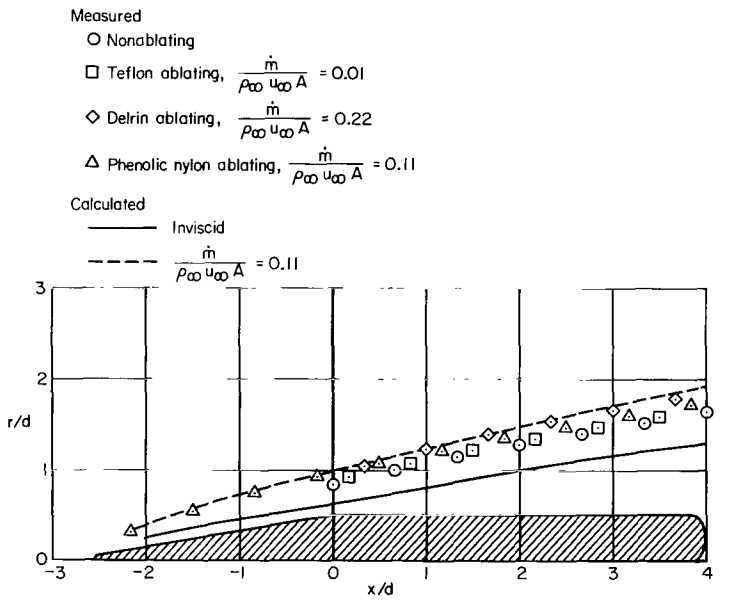

(d) Cone-cylinder, $Re_{\infty,d}$ = 1000.

Figure 4.- The shock shapes for the bodies with ablating noses; M_∞ = 14.

extending the calculations onto the cylinder. This procedure was modified for ablating noses, as will be discussed later. This method was not applied to the cone-cylinder, since according to pictures of the flow of ablation vapors over the corner, using inviscid-wall edge conditions in the boundary-layer calculations resulted in what appeared to be unreasonable growth of the boundary layer behind the nose-cylinder junction. A second viscous-interaction theory was applied to the nonablating bodies in a modified flat-plate analysis that Wagner and Watson (ref. 25) used successfully for predicting the measured pressures on adiabatic-walled cone-cylinders.

The nonablating pressure data in figure 5 agree well with the viscous-interaction calculations at $Re_{\infty,d} = 9000$ (except, perhaps, very near the nose), but are significantly below the viscous-interaction predictions at $Re_{\infty,d} = 1000$. In fact, the pressures on the hemisphere-cylinder at $Re_{\infty,d} = 1000$ are even lower than the theoretical inviscid pressures. This failure of theory to predict surface pressures in the merged-layer regime is similar to a trend previously observed for flat plates, wedges, and cones. The predicted increase of surface pressures at $Re_{\infty,d} = 1000$ is due to the calculated increased shock-layer displacement caused by the boundary-layer growth at that condition. Increased shock-layer displacement, at least over the nose of the cone-cylinder, was verified experimentally by the previous results which showed increased shock-wave displacement for that body at $Re_{\infty,d} = 1000$ (see fig. 3(b)). Thus, the failure of viscous-interaction theory to predict surface pressures at this condition does not appear to be explainable by a decrease in shock-layer displacement on the bodies, as was proposed previously by Kuehn (ref. 10) to explain his data. The explanation for the failure is logically the same as has been verified for sharp bodies; that is, the departure from a Rankine-Hugoniot shock wave upon the merging of the shock wave and the boundary layer within the shock layer. This phenomenon would also explain why Marchand, et al. (ref. 7), measured pressures on blunt cones that were independent of Reynolds number in low-density flow.

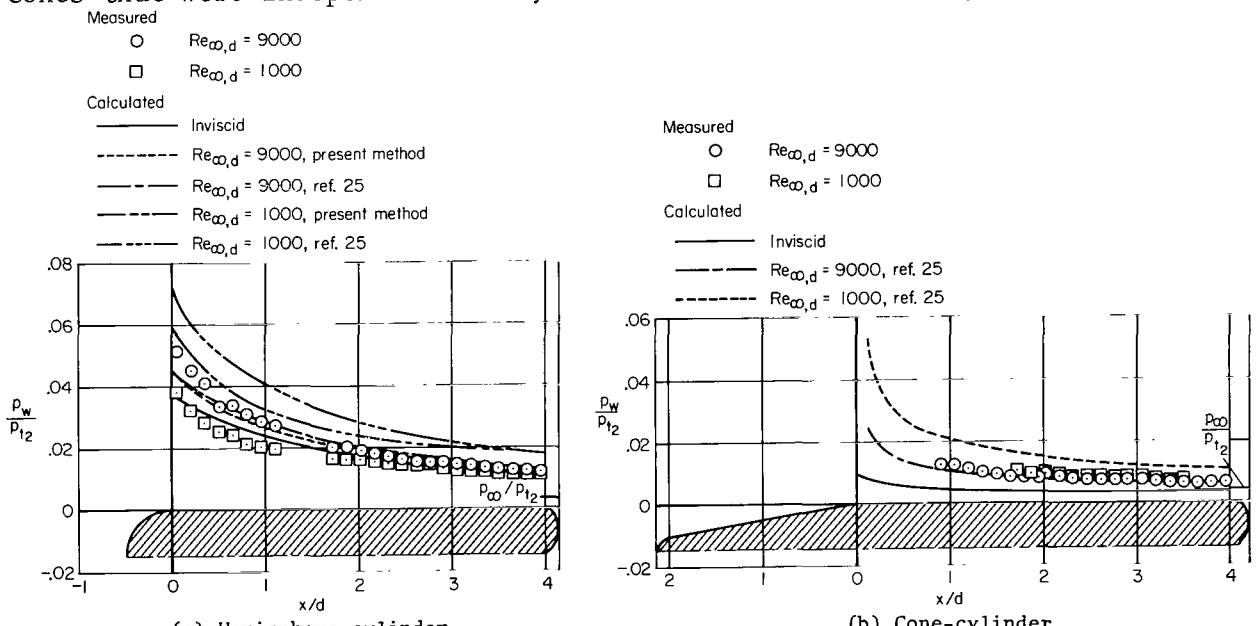

(a) Hemisphere-cylinder. (b) Cone-cylinder.

Figure 5.- The surface pressures for the nonablating bodies; $M_\infty = 14$.

Surface pressure was not measured near the nose of most of the ablating models in figure 6; however, some limited conclusions can be made from available measurements. The predicted viscous induced pressures are presented for some representative hemisphere-cylinders (no method was available for predicting pressures on the cone-cylinder). Since the viscous-interaction theories were shown to fail for the nonablating bodies at $Re_{\infty,d} = 1000$, the theory used here is modified to illustrate better the effects of ablation predicted when the difference between the predicted ablating and nonablating pressures is added to the measured nonablating pressures. The theoretical inviscid pressures are also shown on each figure.

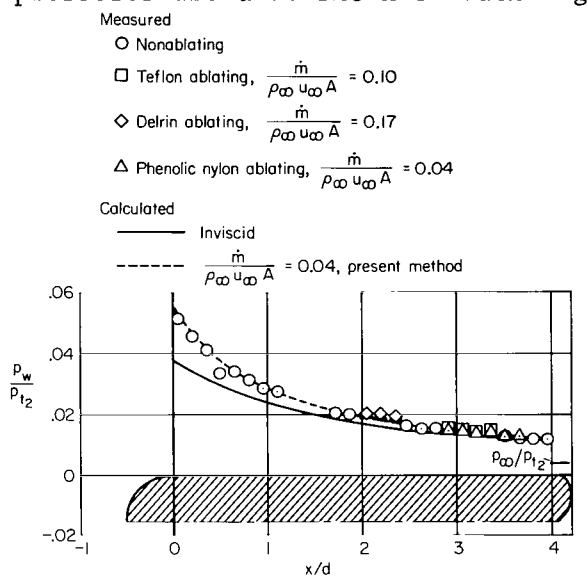

(a) Hemisphere-cylinder, $Re_{\infty,d} = 9000$.

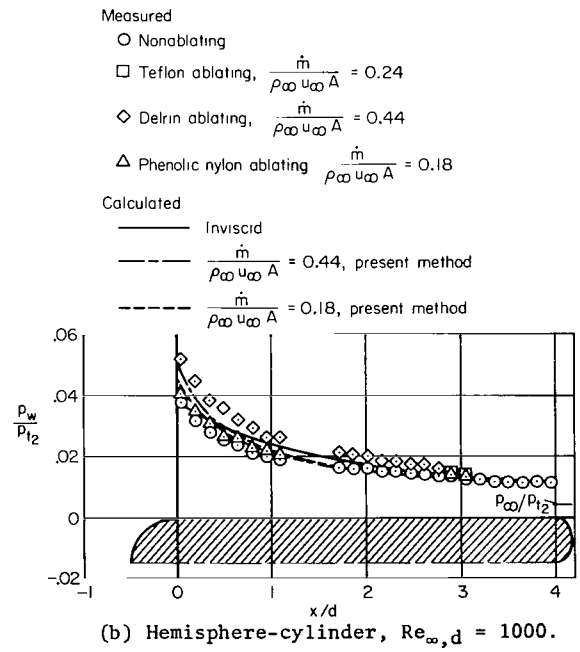

(b) Hemisphere-cylinder, $Re_{\infty,d} = 1000$.

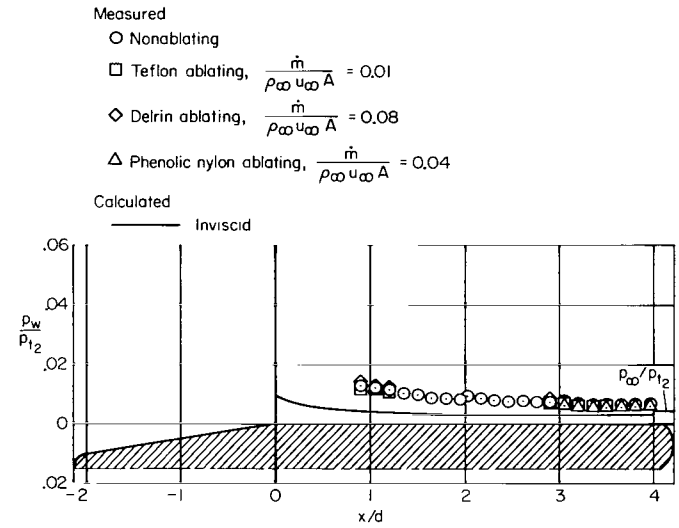

(c) Cone-cylinder, $Re_{\infty,d} = 9000$.

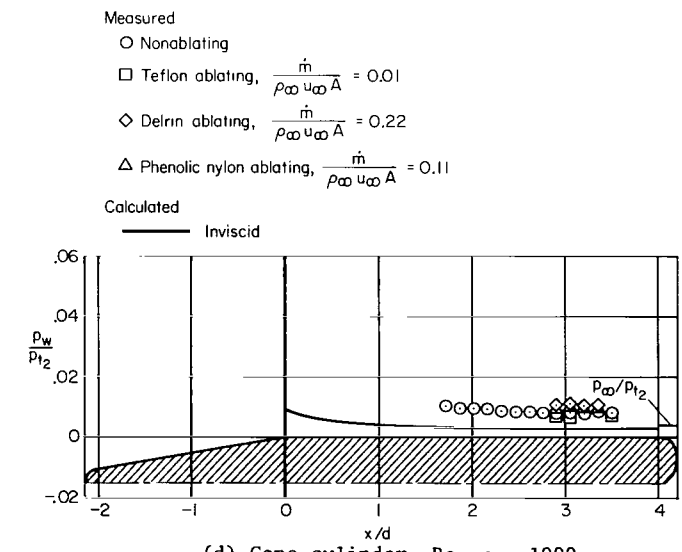

(d) Cone-cylinder, $Re_{\infty,d} = 1000$.

Figure 6.- The surface pressures for the bodies with ablating noses; $M_\infty = 14$.

The pressure data for the bodies at $Re_{\infty,d} = 9000$ (figs. 6(a) and 6(c)) show essentially no effect of nose ablation where measurements were made (beyond two diameters downstream of the nose). The theory for the hemisphere-cylinder agrees with this.

The data for the hemisphere-cylinder at $Re_{\infty,d} = 1000$ (fig. 6(b)) show increased pressures due to ablation just downstream of the nose, but the pressures rapidly approach the nonablating values farther downstream. The cone-cylinder data (fig. 6(d)) also are the same as the nonablating pressures far downstream of the nose, the only region where measurements with ablation were made. The viscous-interaction calculations for the hemisphere-cylinder agree qualitatively with the measured trend, but underpredict the level of the pressures for the Delrin nose. To see if this disagreement was due to blunting of the Delrin hemisphere, a test was made with a nonablating nose having the final shape of the ablated Delrin nose. The measured pressures agreed with the nonablating hemisphere pressures, so the disagreement cannot be attributed to nose blunting.

It thus appears that nose ablation can locally increase surface pressures just downstream of the nose, but the effect does not persist very far downstream. This conclusion would not necessarily apply to entirely ablating bodies.

CONCLUSIONS

From the results of the experiments and comparisons with viscous-interaction theories, the following conclusions were reached:

1. The shock wave for the nonablating hemisphere-cylinder agreed with the predicted inviscid shock wave in both the boundary-layer and merged-layer regimes. The shock wave for the nonablating cone-cylinder was displaced outward from the predicted inviscid shock wave an increasing amount with decreasing Reynolds number over the range tested. Nose ablation displaced the shock waves outward for both bodies. All results were adequately predicted by viscous-interaction theory.

2. The measured surface pressures on the cylinder were greater than the calculated inviscid pressures near the shoulder for both nonablating noses in the boundary-layer regime, but the differences rapidly diminished farther downstream. The results were adequately predicted by either of two viscous-interaction theories. In the merged-layer regime, measured pressures fell much below the predictions of the viscous-interaction theories. This result appears to be due to the merging of the shock wave and boundary layer within the shock layer causing a departure from a Rankine-Hugoniot shock wave. It thus appears that because of merging, highly cooled blunt bodies, at least for the first few nose diameters downstream, will never show the large viscous induced increases in surface pressure that have been measured for adiabatic-walled blunt bodies at higher Reynolds number.

3. Nose ablation in some cases increased cylinder pressures just downstream of the nose, but the effect does not persist very far downstream. These trends were qualitatively predicted by a viscous-interaction method.

Ames Research Center
National Aeronautics and Space Administration
Moffett Field, Calif., 94035, Nov. 26, 1969

REFERENCES

1. Cheng, H. K.: Hypersonic Flow With Combined Leading-Edge Bluntness and Boundary-Layer Displacement Effect. Cornell Aero. Lab. Rep. AF-1285-A-4, Aug. 1960.

2. Horstman, C. C.: Surface Pressures and Shock-Wave Shapes on Sharp Plates and Wedges in Low-Density Hypersonic Flow. Vol. I of Rarefied Gas Dynamics, Academic Press, 1969, pp. 593-605.

3. Kussoy, M. I., and Horstman, C. C.: An Experimental Study of Hypersonic Rarefied Flow Over Sharp Cones. Vol. I of Rarefied Gas Dynamics, Academic Press, 1969, pp. 607-618.

4. Waldron, H. F.: Viscous Hypersonic Flow Over Pointed Cones at Low Reynolds Numbers. AIAA J., vol. 5, no. 2, Feb. 1967, pp. 208-218.

5. McCroskey, W. J.; Bogdonoff, S. M.; and McDougall, J. G.: An Experimental Model for the Sharp Flat Plate in Rarefied Hypersonic Flow. AIAA J., vol. 4, no. 9, Sept. 1966, pp. 1580-1587.

6. Probstein, R. F.: Shock-Wave and Flow Field Development in Hypersonic Re-entry. ARS J., vol. 31, no. 2, Feb. 1961, pp. 185-194.

7. Marchand, E. O.; and Lewis, C. H.: Second-Order Boundary-Layer Effects on a Slender Blunt Cone at Hypersonic Conditions. AIAA Paper 68-54, 1968.

8. Henderson, A., Jr.; Watson, R. D.; and Wagner, R. D., Jr.: Fluid Dynamic Studies to M = 41 in Helium. AIAA J., vol. 4, no. 12, Dec. 1966, pp. 2117-2124.

9. Eaves, R. H., Jr.; and Lewis, Clark H.: Combined Effects of Viscous Interaction and Ideal Source Flow on Pressure and Heat-Transfer Distributions Over Hemisphere Cylinders at $M_\infty \sim 18$. AEDC TR-65-158, July 1965.

10. Kuehn, Donald M.: Experimental and Theoretical Pressures on Blunt Cylinders for Equilibrium and Nonequilibrium Air at Hypersonic Speeds. NASA TN D-1979, 1963.

11. Kuehn, Donald M.; and Monson, Daryl J.: Attached and Separated Boundary Layers on Highly Cooled, Ablating and Nonablating Models at M = 13.8. NASA TN D-4041, 1967.

12. Reinhardt, Walter A.; and Baldwin, Barrett S., Jr.,: A Model for Chemically Reacting Nitrogen-Oxygen Mixtures With Application to Non-equilibrium Air Flow. NASA TN D-2971, 1965.

13. Inouye, Mamoru: Numerical Solutions for Blunt Axisymmetric Bodies in a Supersonic Spherical Source Flow. NASA TN D-3383, 1966.

14. Potter, J. L.; Kinslow, M.; and Boylan, D. E.: An Influence of the Orifice on Measured Pressures in Rarefied Flow. AEDC-TDR-64-175, Sept. 1964.

15. Potter, J. L.; and Bailey, A. B.: Pressures in the Stagnation Regions of Blunt Bodies in Rarefied Flow. AIAA J., vol. 2, no. 4, April 1964, pp. 743-745.

16. Arney, G. D., Jr.; and Bailey, A. B.: An Investigation of the Equilibrium Pressure Along Unequally Heated Tubes. AEDC-TDR-62-26, Feb. 1962.

17. Ahouse, D. R.; and Harbour, P. J.: Flow Field Measurements Upstream of a Blunt Body in a Rarefied Hypersonic Stream. Vol. I of Rarefied Gas Dynamics, Academic Press, 1969, pp. 699-710.

18. Dorrance, W. H.: Viscous Hypersonic Flow, McGraw-Hill Book Co., Inc., N.Y., 1962.

19. Inouye, Mamoru; Rakich, John V.; and Lomax, Harvard: A Description of Numerical Methods and Computer Programs for Two-Dimensional and Axisymmetric Supersonic Flow Over Blunt-Nosed and Flared Bodies. NASA TN D-2970, 1965.

20. Garr, Leonard J.; and Marrone, Paul V.: Inviscid, Nonequilibrium Flow Behind Bow and Normal Shock Waves. Part II. The IBM 704 Computer Programs. Cornell Aero. Lab. Rep. QM-1626-A-12 (II), May 1963.

21. Clutter, Darwin W.; and Smith, A. M. O.: Solution of the General Boundary-Layer Equations for Compressible Laminar Flow, Including Transverse Curvature. Douglas Aircraft Co., Rep. LB 31088. Prepared under Navy Bureau of Naval Weapons, Contract NOw-60-0533-C, Feb. 1963.

22. Wentink, Tunis, Jr.: High Temperature Behavior of Teflon. AFBMD-TN-59-15, July 1959.

23. Lundell, J. H.; Wakefield, R. M.; and Jones, J. W.: Experimental Investigation of a Charring Ablative Material Exposed to Combined Convective and Radiative Heating. AIAA J., vol. 3, no. 11, Nov. 1965, pp. 2087-2095.

24. Hayasi, N.: Displacement Thickness of the Boundary Layer With Blowing. AIAA J., vol. 3, no. 12, Dec. 1965, pp. 2348-2349.

25. Wagner, Richard D., Jr.; and Watson, Ralph: Reynolds Number Effects on the Induced Pressures of Cylindrical Bodies With Different Nose Shapes and Nose Drag Coefficients in Helium at a Mach Number of 24. NASA TR R-182, 1963.

NASA-Langley, 1970 —— 1 A-3499

NATIONAL AERONAUTICS AND SPACE ADMINISTRATION
WASHINGTON, D. C. 20546

OFFICIAL BUSINESS

FIRST CLASS MAIL

POSTAGE AND FEES PAID
NATIONAL AERONAUTICS AND
SPACE ADMINISTRATION

"The aeronautical and space activities of the United States shall be conducted so as to contribute . . . to the expansion of human knowledge of phenomena in the atmosphere and space. The Administration shall provide for the widest practicable and appropriate dissemination of information concerning its activities and the results thereof."

— NATIONAL AERONAUTICS AND SPACE ACT OF 1958

NASA SCIENTIFIC AND TECHNICAL PUBLICATIONS

TECHNICAL REPORTS: Scientific and technical information considered important, complete, and a lasting contribution to existing knowledge.

TECHNICAL NOTES: Information less broad in scope but nevertheless of importance as a contribution to existing knowledge.

TECHNICAL MEMORANDUMS: Information receiving limited distribution because of preliminary data, security classification, or other reasons.

CONTRACTOR REPORTS: Scientific and technical information generated under a NASA contract or grant and considered an important contribution to existing knowledge.

TECHNICAL TRANSLATIONS: Information published in a foreign language considered to merit NASA distribution in English.

SPECIAL PUBLICATIONS: Information derived from or of value to NASA activities. Publications include conference proceedings, monographs, data compilations, handbooks, sourcebooks, and special bibliographies.

TECHNOLOGY UTILIZATION PUBLICATIONS: Information on technology used by NASA that may be of particular interest in commercial and other non-aerospace applications. Publications include Tech Briefs, Technology Utilization Reports and Notes, and Technology Surveys.

Details on the availability of these publications may be obtained from:

SCIENTIFIC AND TECHNICAL INFORMATION DIVISION

NATIONAL AERONAUTICS AND SPACE ADMINISTRATION

Washington, D.C. 20546